A&A 552, A25 (2013)
DOI: 10.1051/0004-6361/201219560

Astronomy & Astrophysics

Detection of a multishell planetary nebula around the hot subdwarf O-type star 2MASS J19310888+4324577

A. Aller[1], L. F. Miranda[1,2], A. Ulla[1], R. Vázquez[3], P. F. Guillén[3], L. Olguín[4], C. Rodríguez-López[1,5], P. Thejll[6], R. Oreiro[5], M. Manteiga[7], and E. Pérez[1]

[1] Departamento de Física Aplicada, Universidade de Vigo, Campus Lagoas-Marcosende s/n, 36310 Vigo, Spain
e-mail: [alba.aller;ulla]@uvigo.es, estherperez@edu.xunta.es
[2] Consejo Superior de Investigaciones Científicas, Serrano 117, 28006 Madrid, Spain
e-mail: lfm@iaa.es
[3] Instituto de Astronomía, Universidad Nacional Autónoma de México, Apdo. Postal 877, 22800 Ensenada, B.C., Mexico
e-mail: [vazquez;fguillen]@astro.unam.mx
[4] Departamento de Investigación en Física, Universidad de Sonora, Blvd. Rosales Esq. L.D. Colosio, Edif. 3H, 83190 Hermosillo, Mexico
e-mail: lorenzo@astro.uson.mx
[5] Instituto de Astrofísica de Andalucía – CSIC, Glorieta de la Astronomía, s/n. 18008 Granada, Spain
e-mail: [roreiro;crl]@iaa.es
[6] Danish Climate Centre at the Danish Meteorological Institute, Lyngbyvej 100, 2100 Copenhagen, Denmark
e-mail: pth@dmi.dk
[7] Departamento de Ciencias de la Navegación y de la Tierra, Universidade da Coruña, Rua de Maestranza, 15001 A Coruña, Spain
e-mail: manteiga@udc.es

Received 8 May 2012 / Accepted 29 January 2013

ABSTRACT

Context. The origin of hot subdwarf O-type stars (sdOs) remains unclear since their discovery in 1947. Among others, a post-asymptotic giant branch (post-AGB) origin is possible for a fraction of sdOs.
Aims. We are involved in a comprehensive ongoing study to search for and to analyze planetary nebulae (PNe) around sdOs with the aim of establishing the fraction and properties of sdOs with a post-AGB origin.
Methods. We used deep Hα and [O III] images of sdOs to detect nebular emission and intermediate-resolution, long-slit optical spectroscopy of the detected nebulae and their sdO central stars. These data were complemented with other observations (archive images, high-resolution, long-slit spectroscopy) for further analysis of the detected nebulae.
Results. We report detecting an extremely faint, complex PN around 2MASS J19310888+4324577 (2M1931+4324), a star classified as sdO in a binary system. The PN shows a bipolar and an elliptical shell, whose major axes are oriented perpendicular to each other, and high-excitation structures outside the two shells. WISE archive images show faint, extended emission at 12 μm and 22 μm in the inner nebular regions. The internal nebular kinematics, which is derived from high-resolution, long-slit spectra, is consistent with a bipolar and a cylindrical/ellipsoidal shell, in both cases with the main axis mainly perpendicular to the line of sight. The nebular spectrum only exhibits Hα, Hβ, and [O III]$\lambda\lambda$4959, 5007 emission lines, but suggests a very low-excitation ([O III]/H$\beta \simeq 1.5$), in strong contrast to the absence of low-excitation emission lines. The spectrum of 2M1931+4324 presents narrow, ionized helium absorptions that confirm the previous sdO classification and suggest an effective temperature $\geq$60 000 K. The binary nature of 2M1931+4324, its association with a complex PN and several properties of the system provide strong support for the idea that binary central stars are a crucial ingredient in the formation of complex PNe.

Key words. planetary nebulae: individual: PNG075.9+11.6 – subdwarfs – stars: individual: 2MASS J19310888+4324577 – binaries: close

1. Introduction

Hot subdwarf O-type stars (sdOs) are low–mass, blue subluminous objects evolving towards the white dwarf phase. In the HR diagram they are located in a region with effective temperature ($T_{\rm eff}$) between $\simeq$40 000 K and $\simeq$100 000 K, and surface gravity ($\log(g)$) between $\simeq$4.0 and $\simeq$6.5. Since their discovery by Humason & Zwicky (1947), the origin of sdOs has been difficult to establish because this region of the HR diagram is crossed by evolutionary tracks of post-asymptotic giant branch (post-AGB), post-red giant branch, and post-extended horizontal branch stars. In addition, binary stars scenarios are also possible (e.g., Napiwotzki 2008; Heber 2009).

The association of sdOs with planetary nebulae (PNe) is essential for obtaining the fraction of sdOs that have a post-AGB origin. As of now, only a few sdO+PN associations have been reported, including the "classical" sdOs LSE 125 and LSS 2018 (Drilling 1983), LSS 1362 (Heber & Drilling 1984), and RWT 152 (Pritchet 1984), as well as several PNe whose central stars have been classified as sdOs (e.g., Rauch et al. 2002; Montez et al. 2010; Weidmann & Gamen 2011). On the other hand, only a few sdOs have been searched for a surrounding PN. Méndez et al. (1988) carried out long-slit spectroscopy of 12 sdOs to search for extended emission. The few detected cases were identified by the authors as diffuse ionized regions in the Galactic disk, and Méndez et al. recommended an image survey to analyze the morphology of the detected extended emissions.

Although morphology should not be used as a unique criterium to identify PNe, it is true that most PNe present axisymmetric shells that are not usually observed in other objects

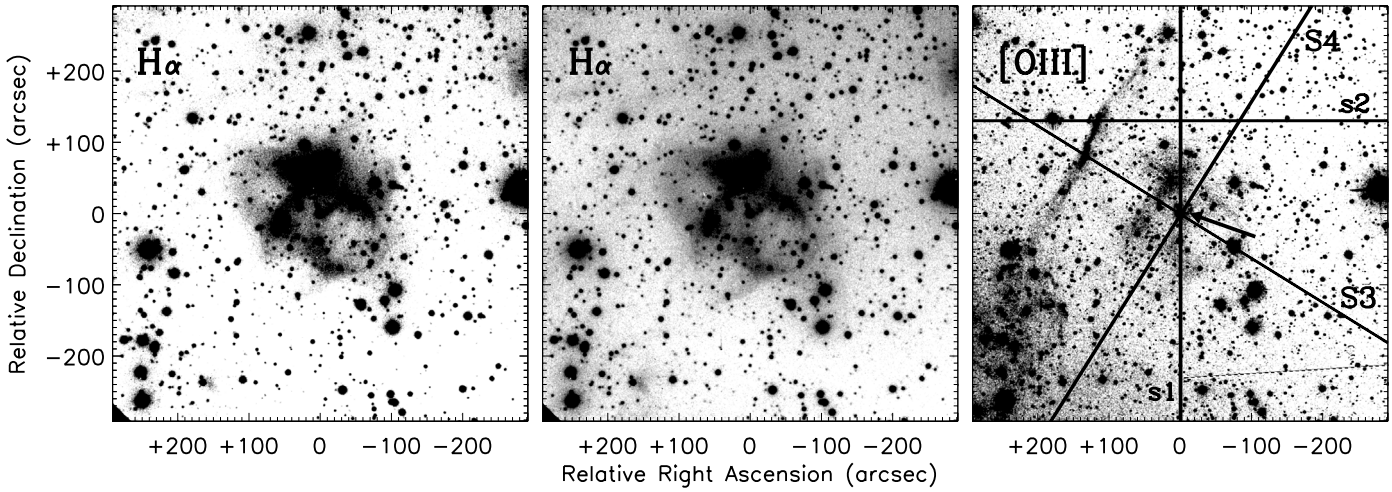

Fig. 1. Gray-scale reproductions of the Hα (*left and center*) and [O III] (*right*) images of 2M1931+4324. Gray levels are linear and two different levels are used to show the Hα image. The slits s1 and s2 (S3 and S4) used for intermediate (high) resolution, long-slit spectroscopy are plotted on the [O III] image (slit width not to scale) in which 2M1931+4324 is also arrowed.

(see, e.g., Miranda et al. 2009). An imaging survey was carried out by Kwitter et al. (1989), who obtained narrow-band images of 14 sdOs (and long-slit spectra of 42 sdOs), although only with a positive and already known detection (RWT 152). We note that the instrumental characteristics of this imaging survey (relatively short exposure times, small field of view) may have prevented them from detecting large and/or very faint PNe. In fact, if sdO+PN associations are common, these PNe should be very faint since only a few can be recognized by a simple visual inspection in the Palomar Observatory Sky Surveys (POSS). Therefore, deeper imaging surveys are required to prove the sdO+PN association.

We are involved in a program to search for and to analyze sdO+PN associations by means of deep direct images and long-slit spectroscopy. In this framework, we present 2MASS J19310888+4324577 (hereafter 2M1931+4324; $\alpha(2000.0) = 19^{\rm h}31^{\rm m}8\overset{\rm s}{.}9$, $\delta(2000.0) = +43°24'58''$; $l = 075\overset{\circ}{.}99$, $b = 11\overset{\circ}{.}6$), which has been spectroscopically classified as an sdO by Østensen et al. (2010). Recently, Jacoby (2011, priv. comm.) and Jacoby et al. (2012) have analyzed photometric *Kepler* data of 2M1931+4324 (Kepler ID 7755741[1]) and find that it is a regular variable with a period of $\lesssim$3 days, suggesting that the star is irradiating a companion. A simple visual inspection of the POSS red and blue plates does not reveal extended emission around 2M1931+4324. However, when the plates are inspected at very low intensity levels, an extremely faint nebulosity around 2M1931+4324 can be suggested. Because of this and the sdO classification, we included 2M1931+4324 in our target list.

In this paper, we present narrow-band optical images that reveal for the first time a very faint multishell PN around 2M1931+4324. We also show mid-infrared images from the WISE archive[2], in which the nebula is detected. Complementary intermediate- and high-resolution, long-slit spectra allow us to confirm the sdO/central star nature of 2M1931+4324, to describe the nebular emission spectrum, and to analyze the internal kinematics of the nebula.

[1] http://archive.stsci.edu/kepler/data_search/search.php

[2] http://irsa.ipac.caltech.edu

2. Observations and results

2.1. Optical imaging

A narrow-band [O III] image was obtained on 2010 August 22 with the Wide Field Camera (WFC) at the 2.5 m Isaac Newton Telescope (INT) on El Roque de los Muchachos Observatory[3] (La Palma, Canary Islands, Spain). The detector was a four 2k × 4k-CCD mosaic with a plate scale of $0\overset{''}{.}33$ pixel^{-1} and a field of view of $34' \times 34'$. We used an [O III] filter (λ_0 = 5008 Å, *FWHM* = 100 Å) to obtain three images with an exposure time of 1800 s each. The sky was clear with an average seeing value of $\simeq 1\overset{''}{.}3$.

A narrow-band Hα image was obtained on 2011 July 12 with the Calar Alto Faint Object Spectrograph (CAFOS) at the 2.2 m telescope on Calar Alto Observatory[4] (Almería, Spain). A SITe 2k × 2k–CCD was used as detector, with a plate scale of $0\overset{''}{.}53$ pixel^{-1} and a circular field of view of $16'$ in diameter. We used an Hα filter (λ_0 = 6563 Å, *FWHM* = 15 Å) to obtain two images of 1800 s and 2400 s. Weather conditions were fair and seeing was $\simeq 2''$. The images were reduced using standard procedures for direct image within the IRAF and MIDAS packages.

Figure 1 shows the Hα and [O III] images of 2M1931+4324 that reveal the existence of a very faint and complex nebula around the star. In Hα two structures can be recognized: a bipolar shell with a size of $\simeq 4\overset{'}{.}3 \times 1\overset{'}{.}7$ and the major axis oriented at position angle (PA) $\simeq$ 55°, and an elliptical shell with a size of $\simeq 5' \times 1\overset{'}{.}8$ and the major axis oriented at PA $\simeq$ 145°. The polar regions of the elliptical shell are very faint and, in fact, the elliptical shell seems to be open. The nebula is particularly bright in the regions where both shells cross each other, while the shells enclose regions of lower intensity. The nebula is very weak in [O III], suggesting low excitation (see Sect. 2.3.2). Additionally, the [O III] image reveals a long filament outside the two shells, which extends from the north towards the southeast of the two shells, ending in a diffuse emission region. While the diffuse

[3] The Isaac Newton Telescope is operated on the island of La Palma by the Isaac Newton Group in the Spanish Observatorio de El Roque de los Muchachos of the Instituto de Astrofísica de Canarias.

[4] The Centro Astronómico Hispano Alemán (CAHA) at Calar Alto is operated jointly by the Max-Planck Institut für Astronomie and the Instituto de Astrofísica de Andalucía (CSIC).

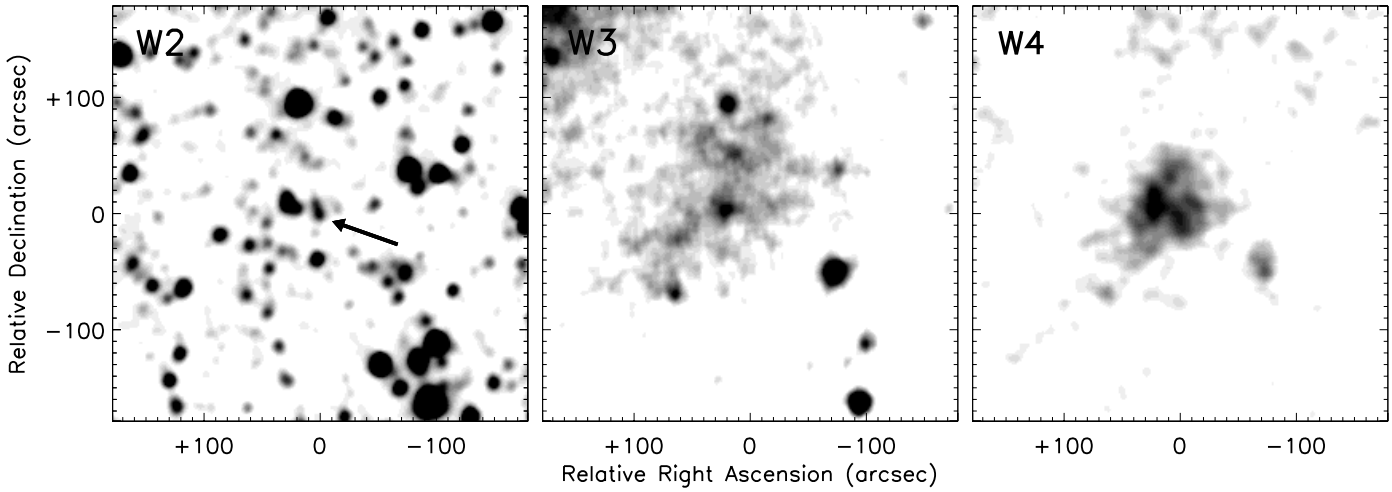

Fig. 2. Gray-scale reproductions of the WISE 2 (4.6 μm), WISE 3 (12 μm), and WISE 4 (22 μm) images of 2M1931+4324. The gray levels are linear and arbitrary, and have been chosen to emphasize the more relevant nebular features. 2M1931+4324 is arrowed in the WISE 2 image, while it is not detected in the WISE 3 and WISE 4 images.

emission could also be present in Hα, the filament is not detected in this line, indicating very high excitation. We note that 2M1931+4324 is not located at the center of the shells but displaced $\simeq$10″ towards PA $\simeq$ 235°, approximately coinciding with the orientation of the minor (major) axis of the bipolar (elliptical) shell. The presence of two axisymmetric shells around a hot sdO star (see Sect. 2.3.1) strongly suggests a PN nature for the nebula. Following the designation scheme for Galactic PNe by Acker et al. (1992), we tentatively propose the name PN G 075.9+11.6 for this nebula, and we refer to it hereafter as such.

2.2. Mid-infrared imaging

To investigate this PN further, we inspected the NASA's Wide-field Infrared Survey Explorer (WISE) database. WISE is a space telescope that is designed to map the entire sky in four infrared bands: 3.4 μm (W1), 4.6 μm (W2), 12 μm (W3), and 22 μm (W4) with angular resolutions of 6.″1, 6.″4, 6.″5, and 12.″0, respectively. Because we are interested in the nebular morphology, we retrieved the W1 to W4 images in the atlas, which have a spatial scale of 1.″375 pixel^{-1}.

Figure 2 shows the W2, W3, and W4 images around 2M1931+4324 (W1 is not shown here). While no nebula can be recognized in the W1 and W2 images, the W3 and W4 ones show nebulous emission that seems to be related to PN G 075.9+11.6. In W3, very weak extended emission is detected in a region of $\simeq$3.′1 × 1.′5 in size oriented at PA $\simeq$ 145°. The orientation is similar to that of the elliptical shell described in Sect. 2.1, although the nebulosity observed in W3 is displaced towards the northeast with respect to the elliptical shell observed in Hα. In W4, extended emission is observed in a region of $\simeq$50″ in size at the center of the nebula, and it presents an irregular, knotty morphology. The origin of the 12 μm and 22 μm emission associated to PN G 075.9+11.6 is difficult to establish without a spectrum. In principle, [S IV] and [Ne III] emission lines could contribute to the emission observed in W3, and [O IV] emission line could be partially included in what is observed in W4 (see Ressler et al. 2010). However, the absence of (prominent) high-excitation emission lines in the optical spectrum (e.g., [Ne III], see Sect. 2.3.2) seems to suggest that the mid-infrared emission is due to cool dust. We also note that 2M1931+4324 itself is detected in W1 and W2, but not in W3 and W4.

To analyze the morphological relationship between the emission observed at 22 μm (W4) and in the optical images, we present a color-composite image obtained by combining Hα, [O III], and W4 in Fig. 3. This image shows that the Hα emission dominates in the bipolar shell and outer regions of the elliptical shell. The [O III] emission comes mainly from the regions where the bipolar and elliptical shells cross each other, and it is the dominant emission in the high-excitation filament and diffuse region. The emission at 22 μm traces only a part of the northwestern border of the elliptical shell, and it is also detected in a region surrounding the central star.

2.3. Intermediate-resolution optical spectroscopy

Intermediate-resolution, long-slit spectra were acquired on 2011 July 13 with CAFOS. Gratings B-100 and R-100 were used to cover the 3200–6200 Å and 5800–9600 Å spectral ranges, respectively, both at a dispersion of $\simeq$2 Å pixel^{-1}. The slit width was 2″, and spectra were obtained at two slit positions: one (denoted s1) with the slit oriented north-south, centered on 2M1931+4324 and with an exposure time of 3600 s for each grism, in order to cover 2M1931+4324 and the brightest nebular regions; and another (s2) with the slit oriented east-west, centered 2.′2 northern of 2M1931+4324 and with an exposure time of 2400 s for each grism, in order to register the outer filament. These slits are also shown in Fig. 1. The spectrophotometric standard HZ 44 was also observed for flux calibration. The sky was clear and seeing was $\simeq$2″. The spectra were reduced using standard procedures for long-slit spectroscopy within the IRAF and MIDAS packages.

2.3.1. The spectrum of 2M1931+4324

Figure 4 shows the optical spectrum of 2M1931+4324. It is dominated by strong ionized helium and hydrogen Balmer absorptions that are blended with the corresponding He II Pickering lines. The narrowness of the absorption lines and the presence of the He IIλ4686 line indicate an sdO nature for 2M1931+4324, in agreement with the classification by Østensen et al. (2010). We also note the presence of N V$\lambda\lambda$4604, 4620 absorption lines that are observed in some sdOs (Husfeld et al. 1989; Rauch et al. 1991). The lack of He Iλ4471 in absorption in the spectrum suggests a $T_{\rm eff} \geq 60\,000$ K (Rauch et al. 1991) and,

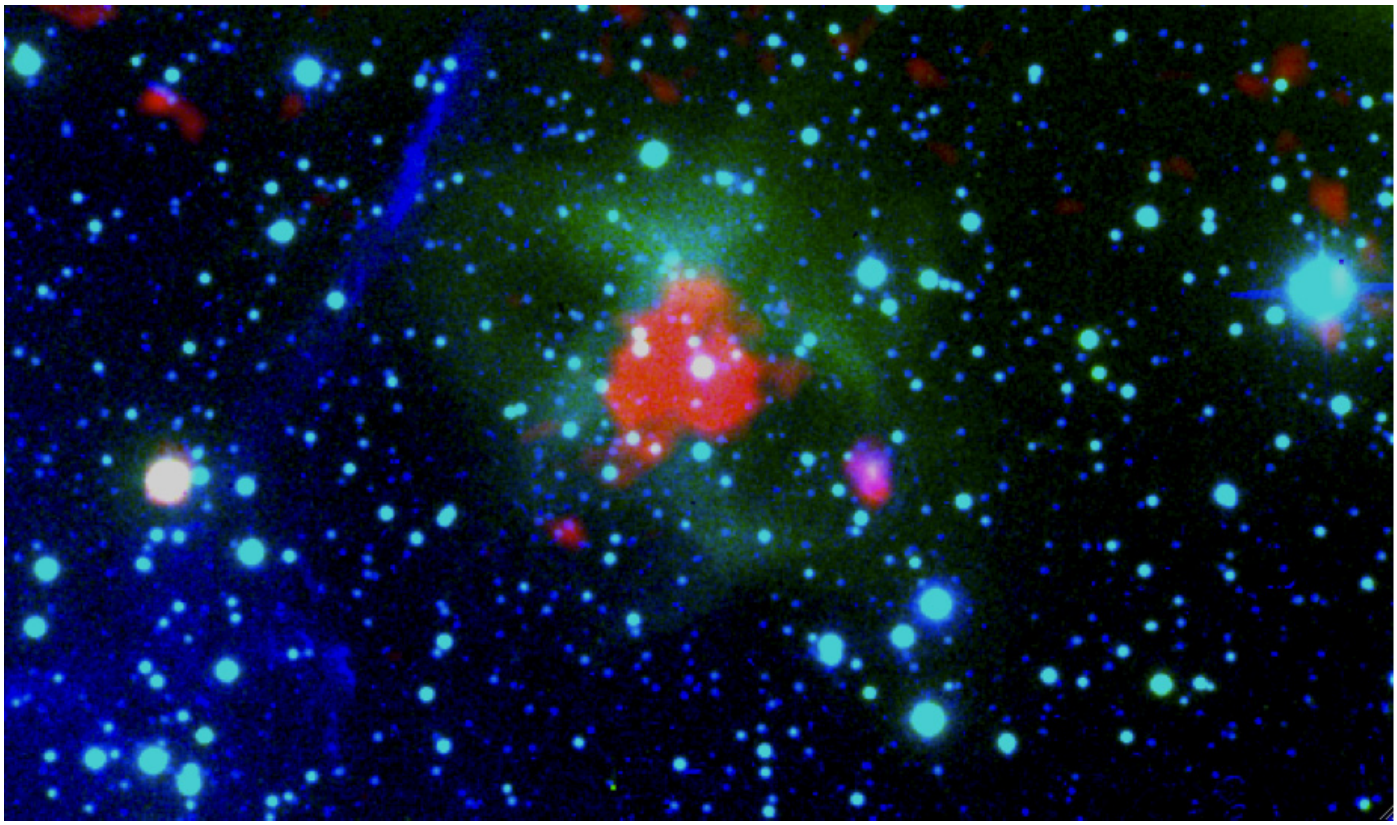

Fig. 3. Color–composite image of PN G 075.9+11.6. Red corresponds to WISE 4 (22 μm), green to Hα, and blue to [O III]. North is up, east to the left. The size of the field shown is 10.′5 × 6.′1. The red knot near the tip of the southwestern bipolar lobe is probably a galaxy that is also observed in the optical images.

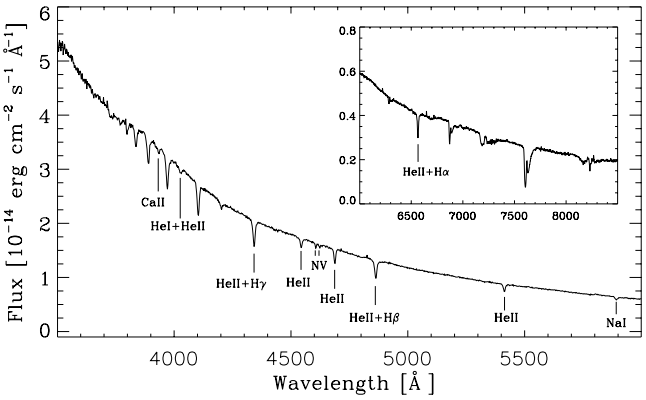

Fig. 4. CAFOS CAHA blue spectrum of 2M1931+4324 in the range 3500–6000 Å. The inset shows the CAFOS CAHA red spectrum. Some helium, hydrogen, and N V absorption lines are indicated, as well as the Ca II λ3968 and Na I λ5895 in absorption.

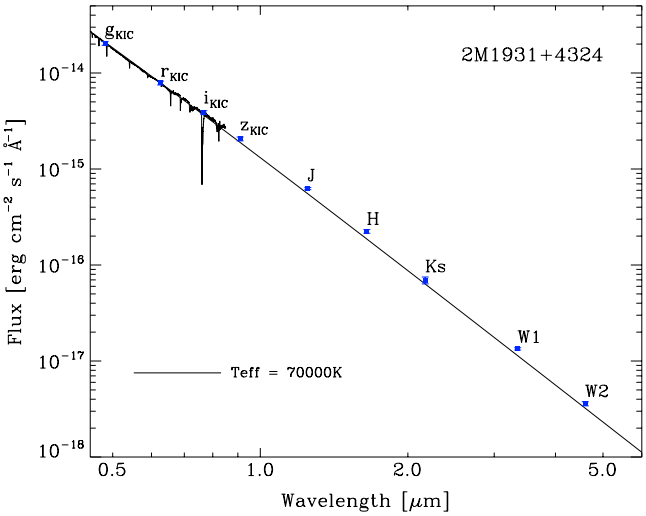

Fig. 5. Spectral energy distribution (SED) of 2M1931+4324 constructed with the magnitudes from the Kepler Input Catalog (KIC), 2MASS Point Source Catalog, and WISE archive. The blue and red CAFOS spectra (see Fig. 4) are also included. The solid line corresponds to a blackbody with $T_{\rm eff}$ = 70 000 K, reddened by A_V = 0.04 (see text) and normalized to the $r_{\rm KIC}$ magnitude.

therefore, that 2M1931+4324 is the central star of the nebula. Finally, a careful inspection of the spectrum reveals Ca II $\lambda\lambda$3934 and Na I $\lambda\lambda$5890, 5895 absorption lines. These absorptions lines could be attributed to a late type companion, although they also are strong features of the interstellar medium. Nevertheless, the reddening towards the object is very low (see Sect. 2.3.2), which seems to favor the first possibility. A radial velocity analysis based on high-resolution spectroscopy of the central star will certainly allow us to decide between these two possibilities.

To obtain more information about 2M1931+4324, we have constructed its spectral energy distribution (SED) with the available photometry: the g, r, i, and z magnitudes from the Kepler Input Catalog (KIC), the J, H, and $K_{\rm s}$ magnitudes from the 2MASS Point Source Catalog[5], and the W1 and W2 magnitudes from the WISE archive. Figure 5 presents the SED,

[5] http://irsa.ipac.caltech.edu

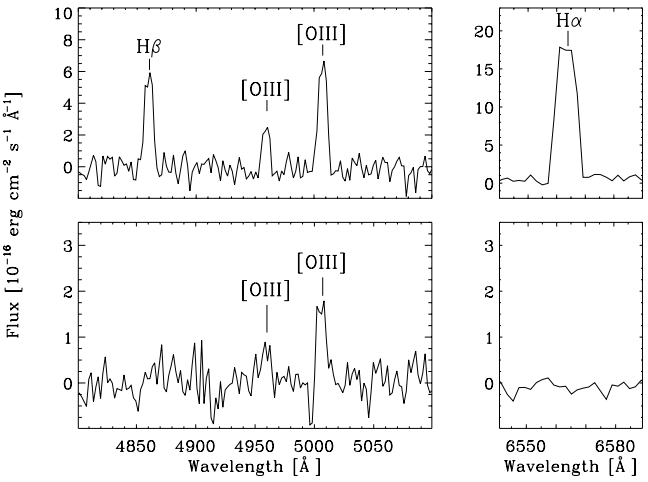

Fig. 6. (*top*) CAFOS CAHA spectra of the detected nebular emission lines from PN G 075.9+11.6. The spectrum has been obtained by integrating the detected emission lines at s1 (see Fig. 1) between 38″ and 75″ north of 2M1931+4324. (*bottom*) Spectrum of the high-excitation filament. The spectrum has been obtained by integrating the detected [O III]λ5007 emission line at s2 (see Fig. 1) in a region of 8″ centered on the filament.

including our optical spectrum. Because the red part of the SED is barely sensitive to $T_{\rm eff}$ for hot central stars, we have plotted in Fig. 5 a blackbody with $T_{\rm eff}$ = 70 000 K, as a guide to what could be expected from extrapolating the stellar continuum of our red spectrum. The blackbody has been reddened by A_V = 0.04 (corresponding to c(Hβ) = 0.02, see Sect. 2.3.2) and normalized at the $r_{\rm KIC}$ magnitude. Figure 5 shows that the KIC, near-, and mid-infrared magnitudes agree reasonably well with those we expected from a blackbody with $T_{\rm eff} \geq$ 60 000 K. Moreover, no noticeable infrared excess can be recognized in the SED of 2M1931+4324. This result seems to rule out a (late type) subgiant or giant as the companion, pointing to other possibilities (e.g., main sequence star, substellar companion). These possibilities should be compatible with the presence of Ca II and Na I absorption lines in the stellar spectrum, if these lines have a stellar origin. A more detailed analysis of the SED will be possible once the atmospheric parameters of 2M1931+4324 have been accurately determined.

2.3.2. The nebular spectrum

In the nebular spectrum obtained at s1 (Fig. 1), only faint Hα, Hβ, and [O III]$\lambda\lambda$4959, 5007 emission lines are detected. Figure 6 presents the integrated spectra around these lines. The underreddened line intensities and their Poissonian errors are listed in Table 1. They have been obtained using the extinction law of Seaton (1979) and a logarithmic extinction coefficient c(Hβ) $\simeq$ 0.02 derived from the observed Hα/Hβ ratio, assuming Case B recombination ($T_{\rm e}$ = 10^4 K, $N_{\rm e}$ = 10^4 cm^{-3}) and a theoretical Hα/Hβ ratio of 2.85 (Brocklehurst 1971).

The [O III]/Hβ line intensity ratio of $\simeq$1.6 (Table 1) indicates a very low-excitation PN. However, the lack of prominent low-excitation emission lines, in particular due to [N II], is highly peculiar. In fact, (low-excitation) bipolar PNe usually present strong [N II] line emission that is not detected from the bipolar shell of PN G 075.9+11.6. It could be that PN G 075.9+11.6 is a density bounded PN with no low-excitation region or a very high-excitation PN with very weak [O III] line emission due to the prevalence of O^{3+} in the nebula. Although the existence of

Table 1. Emission line intensities in PN G 075.9+11.6.

Line	$f(\lambda)$	$I(\lambda)$ I(Hβ) = 100)
H$\beta\lambda$4861	0.000	100 ± 3
[O III]λ4959	−0.023	37 ± 3
[O III]λ5007	−0.034	113 ± 3
H$\alpha\lambda$6563	−0.323	285 ± 4
c(Hβ) = 0.02		
log$F_{\rm H\beta}$(erg cm^{-2} s^{-1} Å^{-1}) = −14.31		

(very) high-excitation is suggested by the outer filament, the absence of other high-excitation emission lines (e.g., He II, [Ar V], [Ne IV]) in the optical spectrum makes these possibilities questionable. Alternatively, the nebula could be strongly deficient in heavy elements. This possibility would be compatible with both low and high excitation in the nebula, and seems to be the only one that accounts for the observed spectrum. A strong deficiency of heavy elements would point to a low-mass progenitor (say, $\leq$1 $M_\odot$; see, e.g., Vázquez et al. 2002) for 2M1931+4324, which would be compatible with the relatively high Galactic latitude of the object (see Stanghellini et al. 2002). A much deeper nebular spectrum is needed to identify more (presumably extremely faint) emission lines and to obtain elemental abundances.

The spectrum of the outer filament obtained at s2 (see Fig. 1) is also shown in Fig. 6. Only very faint [O III]$\lambda\lambda$4959, 5007 line emission is detected (observed [O III]λ5007 flux $\sim$1.7 × 10^{-15} erg cm^{-2} s^{-1} Å^{-1}), confirming its very high-excitation. Similar outer filaments and knots are observed in other PNe (e.g, NGC 40, Balick et al. 1992). In the case of PN G 075.9+11.6, our data do not allow us to establish whether the outer structures are related to mass ejection from 2M1931+4324, or whether they are instead ambient gas ionized by the central star. Nevertheless, we note that the optical and mid-infrared images do not show any nebulosities (except for those detected in our images) in the environment of PN G 075.9+11.6.

2.4. High-resolution spectroscopy

High-resolution, long-slit spectra were obtained on 2012 May 14 and 15 with the Manchester Echelle Spectrometer (Meaburn et al. 2003) at the 2.1 m telescope on the OAN San Pedro Mártir Observatory[6] (Baja California, Mexico). The detector was a 2k × 2k Marconi CCD that was employed with a 4 × 4 binning, resulting in spectral and spatial scales of 0.11 Å pixel^{-1} and 0.″702 pixel^{-1}, respectively. A $\Delta\lambda$ = 90 Å filter was used to isolate the 87th order containing the Hα emission line. The slit (6′ long, 2″ wide) was set on 2M1931+4324 and spectra were obtained at two slit PAs: PA 58° (denoted S3) and PA 148° (S4). These slits are also shown in Fig. 1. In the case of PA 58°, two spectra were secured with the slit on 2M1931+4324 but displaced from each other along PA 58°, and these two spectra were combined in a single long-slit spectrum. Exposure time was 1800 s for each spectrum. A Th-Ar lamp was used for wavelength calibration to an accuracy of ±1 km s^{-1}. The resulting spectral resolution (FWHM) is 12 km s^{-1}. Seeing was $\simeq$2″ during the observations. The spectra were reduced with standard routines for long-slit spectroscopy within the IRAF and MIDAS packages.

[6] The Observatorio Astronómico Nacional at the Sierra de San Pedro Mártir (OAN-SPM) is operated by the Instituto de Astronomía of the Universidad Nacional Autónoma de México.

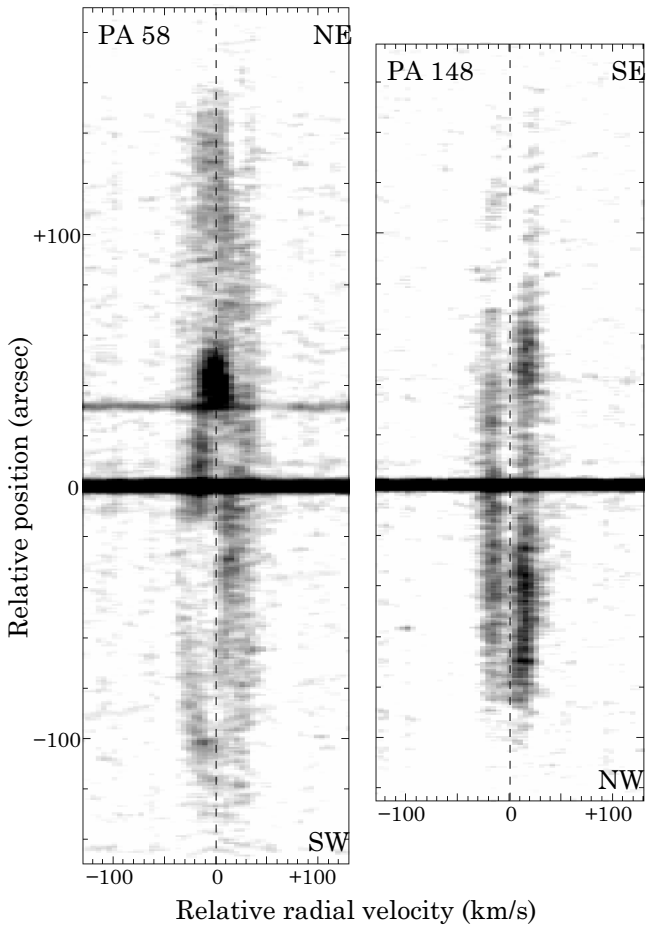

Fig. 7. Gray-scale position-velocity maps of the Hα line observed at two slit position angles (*upper left*). The origin (0, 0) corresponds to the systemic velocity and the position of the central star. The gray-scale is linear. A 3×3 box smooth was used for the representation.

Figure 7 shows position-velocity (PV) maps of the Hα emission line at the two observed PAs. Although the Hα emission is weak, it shows details of the internal kinematics of PN G 075.9+11.6. From the velocity centroid of the line emission feature we derive a heliocentric systemic velocity of $-16 \pm 2\,\mathrm{km\,s^{-1}}$. Internal radial velocities will be quoted hereafter with respect to the systemic velocity.

The PV map at PA 148° (Fig. 7) mainly covers the major axis of the elliptical shell. It shows two extended velocity components with almost constant radial velocities of $\simeq\pm16\,\mathrm{km\,s^{-1}}$. The two components appear mainly parallel to the spatial axis in the PV map, although a slight tilt ($\simeq$1–2 $\mathrm{km\,s^{-1}}$ in $\simeq4'$) could be present with the northwestern (southeastern) region slightly blueshifted (redshifted). The PV map at PA 58° (Fig. 7) covers the major axis of the bipolar shell and shows a more complex kinematics. Two velocity components are observed at the stellar position with radial velocities of $\simeq\pm16\,\mathrm{km\,s^{-1}}$. Towards the southwest, the radial velocity of the two components increases up to $\simeq\pm23\,\mathrm{km\,s^{-1}}$ at $\simeq50''$ from the central star and then it decreases until the two velocity components merge at the systemic velocity, at the southwestern tip of the bipolar shell. An additional, faint velocity component can be identified between $\simeq20''$ and $\simeq80''$ southwestern from the central star, with radial velocities between $\simeq10$ and $\simeq0\,\mathrm{km\,s^{-1}}$, respectively. This component could be related to the elliptical shell or indicate complex motions in the southwestern lobe of bipolar shell. Towards the northeast, up to 35″ from the central star, two velocity components are also recognized with radial velocities of $\simeq-15\,\mathrm{km\,s^{-1}}$ and $\simeq25\,\mathrm{km\,s^{-1}}$. At $\simeq40''$ from the central star, a bright feature is observed at the systemic velocity, which coincides with a bright region observed in the images (Fig. 1) and may correspond to the northeastern edge of the elliptical shell. At angular distances >50″ towards the northeast, the emission feature does not show two velocity components but a single, relatively broad feature mainly at the systemic velocity. This suggests that the northeastern lobe may contain material expanding a lower velocities than the surface of the shell. Finally, the radial velocity of the northeastern tip of the bipolar shell coincides with the systemic velocity.

The kinematics of the elliptical shell observed at PA 148° rules out that this shell corresponds to the projection of a tilted ring, as the images could suggest. If this was the case, one would not detect emission from the inner regions of the shell, but only from the two "points" of the ring intersected by the slit. The possibility of an oblate (equatorial) ellipsoid, such as the one identified in Mz 3 (Guerrero et al. 2004), may also be ruled out because one would expect to see in the PV map at PA 148° decreasing radial velocities from the position of the central star to the tips of the elliptical shell, which is not observed. The presence of two spatially extended velocity components almost parallel to the spatial axis is compatible with a cylindrical (or open ellipsoidal shell) whose major axis is in (or close to) the plane of the sky. The equatorial expansion velocity of this shell is $\simeq16\,\mathrm{km\,s^{-1}}$, and if we assume homologous expansion (velocity proportional to radius), the expansion velocity at the observed maximum size ($\simeq2\farcs5$, see Sect. 2.1) is $\simeq45\,\mathrm{km\,s^{-1}}$. From the equatorial expansion velocity and the equatorial radius of the elliptical shell ($\simeq0\farcs9$, Sect. 2.1), a kinematic age of $\sim1.6\times10^4\times\mathrm{D[kpc]\,yr}$ is obtained for this structure.

The PV map at PA 58°, along the main axis of the bipolar shell, is compatible with the kinematics expected from bipolar motions in an hour-glass-like shell. The main axis of the bipolar shell should be located in the plane of the sky, as indicated by the absence of tilt of the Hα emission feature on the PV map. The equatorial expansion velocity of the bipolar shell is $\simeq16\,\mathrm{km\,s^{-1}}$, while the polar one is $\simeq43\,\mathrm{km\,s^{-1}}$ (also assuming homologous expansion), which are virtually identical to those of the cylindrical shell. From the equatorial expansion velocity and equatorial radius ($0\farcs85$, Sect. 2.1) of the bipolar shell, a kinematic age of $\sim1.5\times10^4\times\mathrm{D[kpc]\,yr}$ is obtained for this structure, which is very similar to that of the cylindrical shell. The kinematic ages of the shells are compatible with an evolved PN. Moreover, the similarity between the kinematic ages suggests that the formation of the two shells has occurred in a short time span, as compared with the age of the nebula.

3. Discussion

The detection of PN G 075.9+11.6 around the sdO/central star 2M1931+4324 adds a new object to the known sample of sdO+PN associations and, therefore, a new sdO whose origin can be ascribed to post-AGB evolution. It is worth noting that 2M1931+4324 is quite bright ($r_{\mathrm{KIC}} \simeq 13\overset{\mathrm{m}}{.}9$) compared to most central stars of PNe. That such a "bright" central star has gone unnoticed to date can be understood by its association with an extremely faint PN that cannot be recognized in the POSS with a simple visual inspection of the plates. In this respect, it should be mentioned that Jacoby et al. (2010) have recently identified a relatively large number of new PNe using the POSS plates, most of them at the detection limit of the plates. It is also noteworthy that PN G 075.9+11.6 and a large fraction of the new PNe identified

by Jacoby et al. (2010) are located at relatively high Galactic latitudes ($|b| > 6°$) and, therefore, cannot be identified in recent PN surveys that are concentrated more towards the Galactic plane (e.g., Parker et al. 2005; Drew et al. 2005). A survey for PNe at higher Galactic latitudes may result in the identification of many new PNe (see Miszalski et al. 2011, and references therein)

The existence of two shells in PN G 075.9+11.6 indicates that complex ejection processes have been involved in the formation of the nebula. As already mentioned, the ejection of the two shells should have occurred in a relatively short time span (as compared with the age of the nebula). Moreover, the location of the two major axes, mainly in the plane of the sky, and the difference of ≃90° in their orientation indicate that the major axes are (virtually) perpendicular to each other. Therefore, the central star has been able to eject two shells in a relatively short time span, including, in addition, a large change of ∼90° in the orientation of the main ejection axis. These results, involving episodic ejections and changes in the orientation of the main ejection axis, are difficult to interpret within a single star scenario but fit in the framework of binary central stars in which they may be explained as a result of stellar interactions, mass transfer, and precession of the collimating agent. In fact, PNe with multiple structures at different orientations, such as quadrupolar or multipolar ones, are usually interpreted invoking a binary central star (e.g., Manchado et al. 1996; Guerrero et al. 2013, and references therein). In this respect, the structure of PN G 075.9+11.6 and the binary nature of 2M1931+4324 (Jacoby et al. 2012) provide support for a binary star scenario in multishell PNe and reinforce the idea that binary stars are an important ingredient in the formation of complex PNe (De Marco 2009, and references therein; Miszalski et al. 2009; Miszalski 2012; Boffin et al. 2012).

Within the context of PNe with binary central stars, we note the off-center position of 2M1931+4324 with respect to the nebular shells. This situation has already been observed in other PNe (e.g., Sahai et al. 1999; Miranda et al. 2001) and interpreted as a result of a possible binary central star (Soker et al. 1998, and references therein). The binary nature of 2M1931+4324 supports this interpretation. Peculiar in PN G 075.9+11.6 is the very large difference between the orientation of the two shells. Other quadrupolar or multipolar PNe do not usually show such large differences in the orientation of the shells (Manchado et al. 1996), although they have been observed in a few cases (see Guillén et al. 2012, and references therein). In an axisymmetric PN with a binary central star, the orientation of the main nebular axis may be expected to be perpendicular to the orbital plane of the binary. If so, the orbital plane of 2M1931+4324 should have been almost parallel to the line of sight (or somewhat tilted, as eclipses are not observed, Jacoby et al. 2012) when each shell was formed, but it has rotated by ∼90° between the ejections. This would imply a dramatic change in the angular momentum of the binary star system, which is not easy to explain. On the other hand, the generation of axisymmetric shells in PNe may be due to other mechanisms (collimated outflows, magnetic fields, see, e.g., Balick & Frank 2002) so that the main nebular axis should not be necessarily related to the orbital plane of a binary central star. Nevertheless, very large changes in orientation of the collimating agent would still be required. In any case, PN G 075.9+11.6 and its binary central star 2M1931+4324 present characteristics that make this system another interesting case for studying the formation of PNe with binary central stars, as, e.g., ETHOS 1 and Fleming 1 (Miszalski et al. 2011; Boffin et al. 2012).

The role of the binary 2M1931+4324 in the formation of PN G 075.9+11.6 could be even more crucial if the nebula is strongly deficient in heavy elements and the central star evolves from a low-mass progenitor, since single stars with low initial mass are expected to form spherical PNe but not axysimmetric and multishell ones (e.g., Vázquez et al. 1999, 2002; Stanghellini et al. 2002, and references therein). Besides obtaining elemental abundances in the nebula, in order to confirm a possible deficiency of heavy elements, estimating the atmospheric parameters of 2M1931+4324 will allow us to constrain the initial mass of the progenitor.

4. Conclusions

Using deep Hα and [O III] images we have detected a very faint nebula around the sdO 2M1931+4324, recently found to be a binary star. The nebula presents a bipolar and an elliptical shell, as well as high-excitation structures outside the two shells. Faint emission from the central nebular regions is also detected at 12 μm and 22 μm in archive WISE images. Analysis of the internal nebular kinematics, by means of high-resolution, long-slit spectroscopy, reveals a bipolar shell and a cylindrical (or open ellipsoidal) shell with their major axes mainly perpendicular to each other. In addition, very similar expansion velocities are found in the two shells that were formed within a relatively short time span.

Our intermediate-resolution spectrum of 2M1931+4324 confirms its sdO classification and indicates a $T_{\rm eff} \geq 60\,000$ K, strongly suggesting a PN nature for the detected nebula that is tentatively referred to as PN G 075.9+11.6. Therefore, 2M1931+4324 adds a new object to the known sdOs associated with a PN and to the sdOs with a post-AGB origin.

The spectrum of PN G 075.9+11.6 exhibits only Hα, Hβ, and [O III] emission lines that indicate a very low-excitation ([O III] to Hβ intensity ratio ≃1.6), in strong contrast to the absence of low-excitation emission lines. The possibility of a very high nebular excitation is difficult to reconcile with the absence of other high-excitation emission lines, suggesting that PN G 075.9+11.6 might be deficient in heavy elements, a fact that should be confirmed by means of very deep spectroscopy and elemental abundance calculations.

The analysis of the spatiokinematical structure of PN G 075.9+11.6 indicates that 2M1931+4324 has been able to eject two axisymmetric shells in a relatively short time span, as compared with the age of the nebula of $\sim 1.6 \times 10^4 \times$ D[kpc] yr, as derived in the present work. Between these two events, the main ejection axis has rotated by ∼90° in such a way that the two main nebular axes are perpendicular to each other and, in both cases, oriented almost in the plane of the sky. The complexity of PN G 075.9+11.6 and the binary nature of 2M1931+4324 provide strong support to the idea that binary central stars are a key ingredient for generating complex PNe.

Acknowledgements. We thank our anonymous referee for his/her comments that have been most helpful for improving the analysis and discussion of the data. We are very grateful to G. Jacoby for sharing with us the result of the binary nature of 2M1931+4324 and for useful comments. We also thank M. Tapia for fruitful comments. This paper has been supported partially by grants AYA 2009-08481, AYA 2009-14648-02, AYA 2011-30147-C03-01, and AYA 2011-30228-C03-01 of the Spanish MINECO, and by grants INCITE09 E1R312096ES, INCITE09 312191PR, and IN845B-2010/061 of Xunta de Galicia, all of them partially funded by FEDER funds. C.R.-L. has a post-doctoral contract with the JAE-Doc program "Junta para la ampliación de estudios" (CSIC) cofunded by FSE, and she acknowledges financial support by grant AYA 2010-14840 of the Spanish MINECO. R.V., L.O., and P.F.G. are supported by PAPIIT-DGAPA-UNAM grant IN109509. L.O. acknowledges support by project PROMEP/103.5/12/3590. Authors also acknowledge the staff at OAN–San Pedro Mártir (particularly to Mr. Gustavo

Melgoza-Kennedy), Calar Alto, and La Palma Observatories for support during observations. This research has made use of the SIMBAD database, operated at the CDS, Strasbourg (France), Aladin, NASA's Astrophysics Data System Bibliographic Services, and the Spanish Virtual Observatory supported from the Spanish MEC through grant AYA2008-02156. This publication makes use of data products from (1) the Wide-field Infrared Survey Explorer, which is a joint project of the University of California, Los Angeles, and the Jet Propulsion Laboratory/California Institute of Technology, funded by the National Aeronautics and Space Administration; (2) from the 2MASS, which is a joint project of the University of Massachusetts and the Infrared Processing and Analysis Center/California Institute of Technology, funded by the National Aeronautics and Space Administration and the National Science Foundation; (3) from the Mikulski Archive for Space Telescopes (MAST). STScI is operated by the Association of Universities for Research in Astronomy, Inc., under NASA contract NAS5-26555. Support for MAST for non-HST data is provided by the NASA Office of Space Science via grant NNX09AF08G and other grants and contracts.

References

Acker, A., Marcout, J., Ochsenbein, F., et al. 1992, Strasbourg-ESO Catalogue of Galactic Planetary Nebulae (Garching, ESO)
Balick, B., & Frank, A. 2002, ARA&A, 40, 439
Balick, B., González, G., Frank, A., & Jacoby, G. 1992, ApJ, 392, 582
Boffin, H. M. J., Miszalski, B., Rauch, T., et al. 2012, Science, 338, 773
Brocklehurst, M. 1971, MNRAS, 153, 471
De Marco, O. 2009, PASP, 121, 316
Drilling, J. S. 1983, ApJ, 270, L13
Drew, J. E., Greimel, R., Irwin, M. J., et al. 2005, MNRAS, 362, 753
Guillén, P. F., Vázquez, R., Miranda, L. F., et al. 2012, MNRAS, submitted
Guerrero, M. A., Chu, Y.-H., Miranda, L. F. 2004, AJ, 128, 1694
Guerrero, M. A., Miranda, L. F., Ramos-Larios, G., & Vázquez, R. 2013, A&A, 551, A53
Heber, U. 2009, ARA&A, 47, 211
Heber, U., & Drilling, J. S. 1984, Mitt. Astron. Ges. Hamburg, 62, 252
Humason, M. L., & Zwicky, F. 1947, ApJ, 105, 85
Husfeld, D., Butler, K., Heber, U., & Drilling, J. S. 1989, A&A, 222, 150
Jacoby, G. H., Kronberger, M., Patchick, D., et al. 2010, PASA, 27, 156
Jacoby, G., de Marco, O., Howell, S., & Kronberger, M. 2012, AAS Meeting, 219, 418.02
Kwitter, K. B., Congdon, C. W., Pasachoff, J. M., & Massey, P. 1989, AJ, 97, 1423
Manchado, A., Guerrero, M. A., Stanghellini, L., & Serra-Ricart, M. 1996, The IAC Morphological Catalog of Galactic Planetary Nebula (La Laguna, Instituto de Astrofísica de Canarias)
Meaburn, J., López, J. A., Gutiérrez, L., et al. 2003, Rev. Mex. Astron Astrofis., 39, 185
Méndez, R. H., Gathier, R., Simon, K. P., & Kwitter, K. B. 1988, A&A, 198, 287
Miranda, L. F., Torrelles, J. M., Guerrero, M. A., Vázquez, R., & Gómez, Y., 2001, MNRAS, 321, 487
Miranda, L. F., Pereira, C. B., & Guerrero, M. A. 2009, AJ, 137, 4140
Miszalski, B. 2012, in Planetary nebulae: an eye to the future (Cambrige University Press), IAU Symp., 283, 107
Miszalski, B., Acker, A., Parker, Q. A., & Moffat, A. F. J. 2009, A&A, 505, 249
Miszalski, B., Corradi, R. L. M., Boffin, H. M. J., et al. 2011, MNRAS, 413, 1264
Montez, R., De Marco, O., Kastner, J. H., & Chu, Y.-H. 2010, ApJ, 721, 1820
Napiwotzki, R. 2008, in Hot Subdwarf Stars and Related Objects, eds. U. Heber, S. Jeffery, & R. Napiwotzki, ASP Conf. Ser., 392, 139
Parker, Q. A., Phillipps, S., Pierce, M. J., et al. 2005, MNRAS, 362, 689
Østensen, R. H., Silvotti, R., Charpinet, S., et al. 2010, MNRAS, 409, 1470
Pritchet, C. 1984, A&A, 139, 230
Rauch, T., Heber, U., Hunger, et al. 1991, A&A, 241, 457
Rauch, T., Heber, U., & Werner, K. 2002, A&A, 381, 1007
Ressler, M. E., Cohen, M., Wachter, S., et al. 2010, AJ, 140, 1882
Sahai, R., Dayal, A., Watson, A. M., et al. 1999, AJ, 118, 468
Seaton, M. J. 1979, MNRAS, 187, 73
Soker, N., Rappaport, S., & Harpaz, A. 1998, ApJ, 496, 842
Stanghellini, L., Villaver, E.,Manchado, A., & Guerrero, M. A. 2002, ApJ, 576, 285
Vázquez, R., López, J.A., Miranda, L. F., et al. 1999, MNRAS, 308, 939
Vázquez, R., Miranda, L. F., Torrelles, J. M., et al. 2002, ApJ, 576, 860
Weidmann, W. A., & Gamen, R. 2011, A&A, 526, A6